Sensors and Actuators B 246 (2017) 1049–1055

Contents lists available at ScienceDirect

Sensors and Actuators B: Chemical

journal homepage: www.elsevier.com/locate/snb

Pressed region integrated 3D paper-based microfluidic device that enables vertical flow multistep assays for the detection of C-reactive protein based on programmed reagent loading

Juhwan Park, Je-Kyun Park*

Department of Bio and Brain Engineering, Korea Advanced Institute of Science and Technology (KAIST), 291 Daehak-ro, Yuseong-gu, Daejeon 34141, Republic of Korea

ARTICLE INFO

Article history:
Received 1 November 2016
Received in revised form 6 February 2017
Accepted 24 February 2017
Available online 1 March 2017

Keywords:
3D Paper-based microfluidics
C-Reactive protein
Pressed paper
Vertical flow assays

ABSTRACT

Although vertical flow assays (VFAs) have a number of advantages compared to lateral flow assays (LFAs) such as a short analysis time, no line interference, and no Hook effect, VFAs are not preferred as LFAs because of their complicated operation principle. In this study, we demonstrated VFAs with multistep reactions for the detection of C-reactive protein (CRP) based on the programmed reagent loading in a pressed region integrated 3D paper-based microfluidic device. The flow order of all reagents in a 3D paper-based microfluidic device was programmed based on the delayed flow caused by the pressed region as well as the geometry modification of the paper channel. After simultaneous loading of all the reagents required for assays, they are sequentially loaded into the analysis region with a programmed sequence. As a proof of concept, a high-sensitivity CRP (hs-CRP) detection with signal amplification was performed to predict the riskiness of cardiovascular disease within 15 min. The detection limit was improved from 0.01 to 0.005 μg/mL via a maximum 3.47-fold signal amplification. Additionally, the upper limit of hs-CRP detection increased to 5 μg/mL without Hook effect. Finally, we successfully detected hs-CRP in a clinically relevant range (0.005–5 μg/mL), while LFAs cannot cover due to the Hook effect.

1. Introduction

C-Reactive protein (CRP) that produced in the liver has been widely used as an indicator of inflammation. During the inflammation responses, the concentration of CRP increases up to 200 μg/mL and many approaches for monitoring the inflammation responses have been reported by measuring the CRP concentration [1]. It is also known that the CRP concentration under the normal range can be a potential indicator of cardiovascular disease [2]. The risk of cardiovascular disease, according to the concentration of CRP, is low below 1 μg/mL, moderate from 1 to 3 μg/mL, and high over 3 μg/mL [3]. Therefore, a high-sensitivity CRP (hs-CRP) detection under the clinically relevant CRP concentration range (0–5 μg/mL), including a clinical cutoff concentration (1 and 3 μg/mL), is highly desirable to predict the risk of cardiovascular disease. Many approaches for hs-CRP detection have been developed, including the commercialized methods [4,5], the microfluidic systems [6,7], and other complicated methods [8,9].

Paper materials have been widely used as a platform for point-of-care testing (POCT) because of their wide availability, low cost, and user-friendliness [10]. Among a number of paper-based POCT platforms, lateral flow assays (LFAs) have been generally used for analyzing the concentration of various target molecules including CRP [11–13]. As alternatives to LFAs, vertical flow assays (VFAs), also known as flow-through assays in which the flows pass through a test region vertically, have many advantages over LFAs [14,15]. First, compared with LFAs, VFAs have a relatively short analysis time due to their short fluid path. Second, there is no Hook effect in VFAs because target analytes and detection conjugates flow sequentially into the test region. On the contrary, target analytes and detection conjugates do not sequentially flow into the test region in LFAs, resulting in a decrease in the signal intensity at the high concentration of target analytes [16]. Excess target analytes that do not bind to the detection conjugates may interfere with the interaction between detection conjugates bound target analytes and capture antibodies (Abs). Third, it is easy to expand into the multiple detection format by adding additional test regions without interference among the test regions. The signal intensity in LFAs may be affected by the position of the test line because the detection conjugates pass through each test line one by one.

* Corresponding author.
E-mail address: jekyun@kaist.ac.kr (J.-K. Park).

http://dx.doi.org/10.1016/j.snb.2017.02.150
0925-4005/

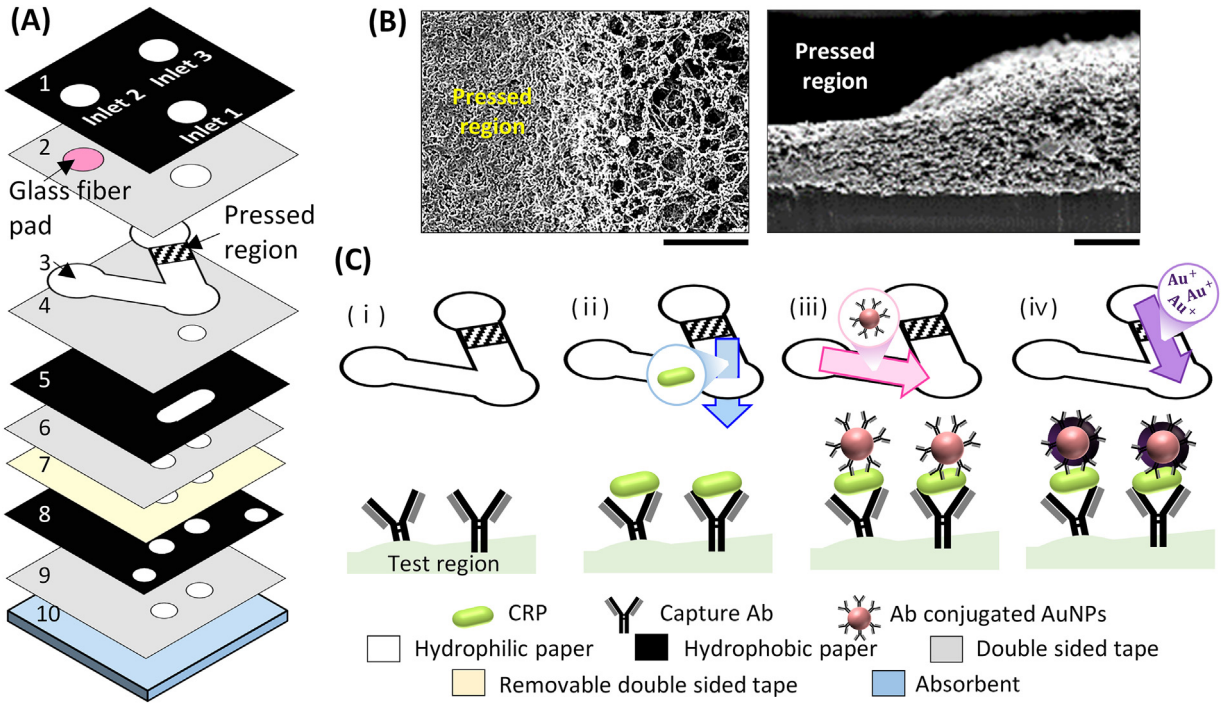

Fig. 1. Device configuration and operation principle. (A) Schematic of a pressed region integrated 3D paper-based microfluidic device for VFAs with multistep reactions, which is assembled using patterned double sided tapes (2nd, 4th, 6th, and 9th layers). (B) Top and side view of SEM images for the pressed paper which was pressed with 49.2 MPa. Scale bars = 50 μm. (C) Operation principle of VFAs with multistep reactions based on the programmed reagent loading.

Although VFAs have a number of advantages over LFAs, they are not favorable than LFAs because of their complicated operation principle that requiring the manual sequential loading of multiple reagents (target analytes, wash buffer, detection conjugates, etc.). To compensate this user-unfriendliness of VFAs, improved versions such as a one-step VFAs [17], a 3D paper architecture based VFAs [18], and a lab-in-a-syringe [19] have been recently reported. They simplified the complicated operation principle of VFAs by allocating detection conjugates in the middle of the flow path of the target analytes, but this flow mechanism, which involves the pre-mixing of detection conjugates and target analytes bound to the capture Abs, can decrease the overall signal intensity at the test region [20]. In other words, the flow mechanism that allows the sequential delivery of target analytes and detection conjugates into the capture Abs is beneficial for acquiring a higher signal intensity. Additionally, they are limited to a single step reaction that cannot handle multistep assays for the higher signal intensity. The high signal intensity plays an important role for the higher sensitivity of assays and can widen the detection range of target analytes by an improvement in the detection limit.

On the other hand, many kinds of microfluidic paper-based analytical devices that enable sequential delivery of each reagent (target analytes, detection conjugates, additional reagents, etc.) into the test region after simultaneous loading of reagents have been developed by controlling the capillary flow [21–23]. However, because they use a lateral flow for the delivery of all the reagents required for assays they require a quite long analysis time. In addition, they are spatially limited to integrate additional fluidic channels for specific functions. Meanwhile, 3D paper-based microfluidic devices using a combination of lateral and vertical flows offer many advantages for the handling of various assay types [24]. The combination of lateral and vertical flows in a 3D paper-based microfluidic device can realize a shorter analysis time and spatially unlimited integration of fluidic channels or specific functions. Although 3D paper-based microfluidic devices offer many advantages to handle many kinds of assays as mentioned above, many previous studies have concentrated on fabrication methods and device packaging [25–27]. Therefore, more methods to control capillary flow in 3D paper-based microfluidic devices such as a paper-based fluidic timer [28] and a 3D paper-based slip device [29] should be developed to make the best use of 3D paper-based microfluidic devices.

Here, we present VFAs with multistep reactions based on the programmed reagent loading using a pressed region integrated 3D paper-based microfluidic device. Recently, we have developed a pressed paper and applied it for the sequential delivery of multiple reagents in LFAs with multistep reactions [30,31]. In this work, the pressed region was integrated into a 3D paper-based microfluidic device to simplify the complicated operation principle of VFAs with multistep reactions based on the delayed flow. The reagent loading order was programmed by controlling the amount of applied pressure as well as the geometry of the paper channel. By loading all the reagents at the same time, each reagent was loaded into the analysis region in the programmed order. The complicated operation principle of VFAs with multistep reactions was simplified by maintaining the reagent loading mechanism of conventional VFAs, enabling analysis for a wide range of target analytes without Hook effect. Additionally, the sensitivity of assays was improved by exploiting multistep reactions for signal amplification. Finally, we performed hs-CRP detection with signal amplification for the prediction of cardiovascular disease in a clinically relevant rage (0.005–5 μg/mL) without Hook effect.

2. Material and methods

2.1. Materials

Anti-CRP monoclonal Abs produced in mouse (ab8278) and polyclonal Abs produced in rabbit (ab31156) were purchased from Abcam (Cambridge, UK). Human native CRP (30-AC05S) was purchased from Fitzgerald (North Acton, MA, USA). Anti-rabbit IgG Abs, 20 nm diameter gold nanoparticles (AuNPs), and Tween-20

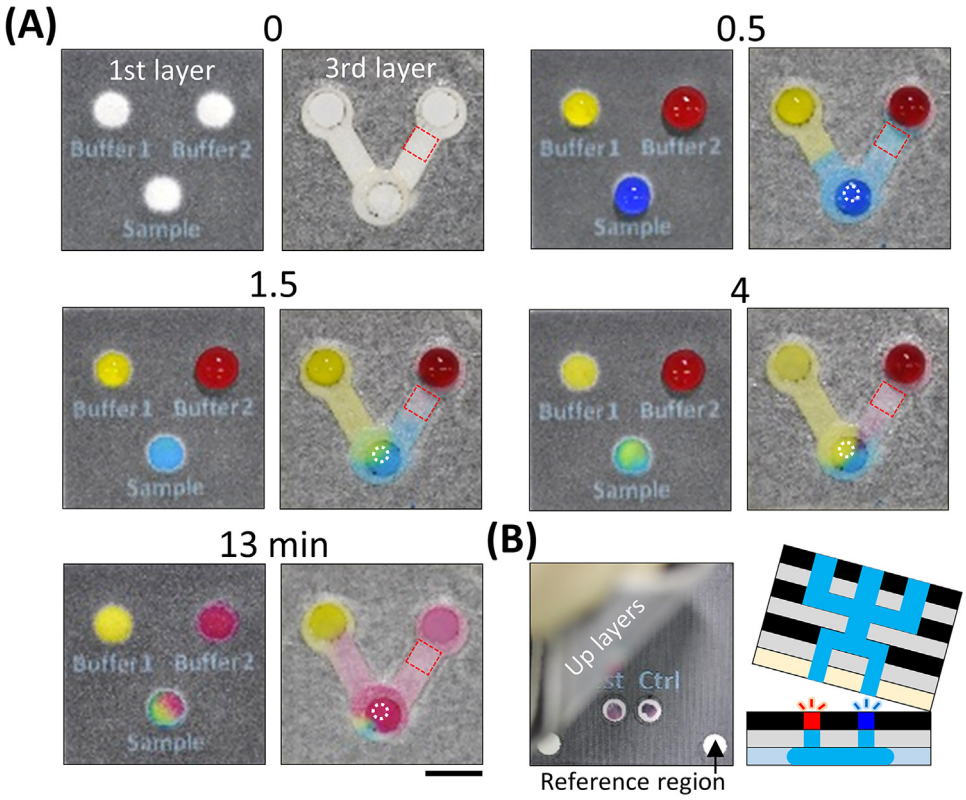

Fig. 2. Detection process of VFAs with multistep reactions. (A) Flow demonstration with three kinds of food dyes at the 1 st and 3rd layer after simultaneous loading of all reagents. White dotted circles indicate the paper disk at the 4th layer and dotted boxes indicate the pressed region. Scale bar = 5 mm. (B) The final detection signals are easily observable by lifting up the 1st–7th layers.

were purchased from Sigma-Aldrich (St. Louis, MO, USA). Bovine serum albumin (BSA) was purchased from Santa Cruz Biotechnology (Santa Cruz, CA, USA). A gold enhancer solution was purchased from Nanoprobes (Yaphank, NY, USA). 15 μm pore size nitrocellulose (NC) membrane, including transparent polyester backing (thickness = 207 μm) (CNPC-SS12) for the fabrication of pressed paper, was purchased from Advanced Microdevices (Ambala Cantt, India). 1 Chr chromatography paper (thickness = 180 μm) (3001-917) and 0.45 μm pore size NC membrane (10600002) for the analysis region were purchased from GE Healthcare Life Sciences (Seoul, Korea). Absorbent pad (grade 222) and sample pad (grade 319) were purchased from Ahlstrom (Helsinki, Finland). Glass fiber pad (GFCP103000) was purchased from Millipore (Billerica, MA, USA). Wax printing patterns were designed with Microsoft PowerPoint and laser cutting patterns were designed with AutoCAD.

2.2. AuNPs functionalization with Abs

750 μL AuNPs solution was mixed with 10 μg anti-CRP polyclonal Abs and incubated for 20 min. Then 100 μL of 3% BSA in distilled water was added to block the surface of AuNPs. After 20 min of incubation, the supernatant was removed after 30 min of centrifugation at 8700 rpm at 4 °C. Finally, Ab-functionalized AuNPs were re-suspended with a desired volume of 1% BSA and 0.01% Tween-20 in phosphate buffered saline (PBS).

2.3. 3D paper architecture for calibration of delayed flow

15 μm pore size NC membrane and double sided tapes were cut into a pre-designed shape with a CO_2 laser cutter (C40-60W; Coryart, Anyang, Korea). The NC membrane was partially pressed with an acrylic plate (2 mm × 3 mm) using a press machine (SWP-HP180-120S; Sam Woo, Siheung, Korea). The amount of the applied pressure was measured by placing a load cell (CLS-1T; Curiosity Technology, Paju, Korea) under the press machine. Because there is a plastic backing at 15 μm pore size of the NC membrane, it was modified by conjugation with 1 Chr chromatography paper to adjust a pressed paper into a 3D paper architecture (Fig. S1), which can be used to facilitate the mass transfer between vertically-assembled papers. Inlet and outlet layers composed of 1Chr chromatography paper were patterned using a wax printer (ColorQube 8570, Xerox, Japan). The patterned papers were incubated on 150 °C hot plate for 3 min. The holes of double sided tapes were filled with a paper disk obtained by CO_2 laser cutting of 1Chr chromatography paper. Blue dye was pre-loaded and dried in the paper disk (near the outlet). The 3D paper architecture was assembled by connecting paper layers with shaped double sided tapes. The detailed dimensions of each layer during the design process are shown in Fig. S2. 7 μL of distilled water was loaded into the inlet and the time at which the blue color appeared at the outlet was measured.

2.4. Fabrication of LFA strips

1 mg/mL of anti-CRP monoclonal Abs and anti-rabbit IgG Abs were dispensed on a 15 μm pore size NC membrane for the test and control lines using a dispenser (LPM-02; Advanced Microdevices). After drying it in a desiccator, it was cut into a strip (4 mm × 25 mm). To prevent non-specific binding of molecules, each strip was blocked with 10 μL of 1% BSA and 0.01% Tween-20 in PBS. 15 μL of Ab-functionalized AuNPs re-suspended in 750 μL were loaded into a glass fiber pad (4 mm × 10 mm) and dried in a desiccator. Finally, the NC membrane strip, the glass fiber pad, the absorbent pad (4 mm × 20 mm), and the sample pad (4 mm × 15 mm) were

assembled on an adhesive plastic backing by overlapping about 2 mm.

2.5. Device configuration and fabrication

The device is composed of wax-printed 1 Chr chromatography papers (1st and 5th layer), double sided tapes (2nd, 4th, 6th, and 9th layer), pressed paper (3rd layer), removable double sided tape (7th layer), wax-printed 0.45 μm pore size NC membrane (8th layer), and absorbent pad (10th layer) (Fig. 1A). Double sided tape and removable double sided tape were cut into a pre-designed shape with a CO_2 laser cutter. The 1st, 5th, and 8th layers were patterned by printing desired patterns with a wax printer and incubated them on a hot plate of 150 °C for 3 min. Holes in the double sided tapes were filled with a paper disk made of 1 Chr chromatography paper. Holes in the removable double sided tape were filled with a paper disk of 0.45 μm pore size NC membrane to generate a uniform signal at the analysis region instead of a paper disk of 1Chr chromatography paper showing rough surface properties (Fig. S3). Paper disks were obtained with a desirable shape using a CO_2 laser cutter. For the 3rd layer, a 15 μm pore size NC membrane was partially pressed using a press machine with an optimized amount of pressure after cutting into a pre-designed shape with a CO_2 laser cutter. Then it was modified to generate a vertical flow by conjugating the paper disk of 1 Chr chromatography paper. The detailed dimensions of each layer during the design process are shown in Fig. S4. There is an analysis region in the 8th layer that includes test and control. Test region exhibits the results of the assay and control region indicates a good operation of the device. 0.3 μL of anti-CRP Abs (1 mg/mL) and anti-rabbit IgG Abs (1 mg/mL) were dispensed at the test and control region, respectively. To prevent non-specific binding of molecules, the 1st–7th layers were partially blocked with 1% BSA in PBS. To facilitate the reagent loading process, Ab-functionalized AuNPs were stored in the device with a dried form. 3 μL of Ab-functionalized AuNPs re-suspended in 37.5 μL was loaded into a glass fiber pad disk and dried in a desiccator. Finally, the device for VFAs with multistep reactions was completed by assembling each layer.

2.6. Analysis of detection results

The sample solution was prepared by diluting human native CRP with PBS into a desired concentration. For LFAs, 80 μL sample solution was loaded into the sample pad. After 15 min, the colorimetric signal at the test line in LFA strip was captured with a digital camera. The signal intensity of the test line was normalized by subtracting the signal intensity of the bare NC membrane strip with the ImageJ software. For the VFAs with multistep reactions, 20 μL of sample solution, 10 μL of rehydration buffer (1% BSA in PBS), and 20 μL of the prepared gold enhancer solution were simultaneously loaded into the inlet 1–3, respectively. After 15 min, the colorimetric signal at the test region was captured with a digital camera after removing the 1st–7th layers. The signal intensity of the test region was normalized by subtracting the signal intensity of the reference region with the ImageJ software. The signal intensity at the detection limit was calculated by the sum of the signal intensity at the blank and the threefold standard deviation at the blank.

3. Results and discussion

3.1. Operation principle

There are three inlets for reagent loading in a pressed region integrated 3D paper-based microfluidic device for VFAs with multistep reactions. The inlet 1 has a short fluid path to an analysis region compared to that of the inlets 2 and 3 so that the reagent from

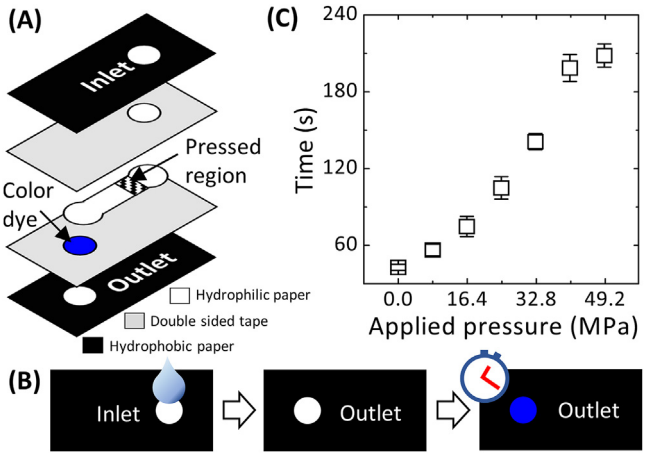

Fig. 3. Calibration of the delayed flow. (A) Schematic of a simple 3D paper-based microfluidic device for calibrating delayed flow. (B) Schematic of operation principle for the calibration of delayed flow. (C) The time at which the blue color appeared in the outlet was plotted with respect to the increasing amount of applied pressure. (For interpretation of the references to colour in this figure legend, the reader is referred to the web version of this article.)

the inlet 1 passes first through the analysis region. The fluid path from the inlet 3 has a pressed region that exhibit decreased porosity, permeability, and thickness while the fluid path from the inlet 2 does not include a pressed region (Fig. 1B). The pressed region plays a role as a fluid resistance so that the reagent from the inlet 2 passes through the analysis region before the reagent from the inlet 3 reaches at the analysis region. Therefore, CRPs as target analytes first pass through the analysis region and are captured by anti-CRP Abs in the test region. After that, dried Ab-conjugated AuNPs are rehydrated by buffer from the inlet 2 and they detect captured CRPs at the test region. For signal amplification, the prepared gold enhancer solution from the inlet 3 amplifies the signals at the analysis region by attaching gold ions at the surface of the AuNPs (Fig. 1C). As shown in Fig. 2A, a whole detection process can be performed by simultaneous loading of all the reagents. Then, each reagent from the inlets 1–3 was programmed to be sequentially loaded into the analysis region. Finally, the detection results were easily observable by lifting the 1st–7th layers over the analysis region (Fig. 2B). We facilitated the removal of the 1st–7th layers using a removable adhesive tape as the 7th layer. Furthermore, there is no concern about the evaporation of the reagent during the detection process at the analysis region as it is covered with a flow control layer.

3.2. Calibration of delayed flow in a 3D paper-based microfluidic device

When NC membrane is exposed to pressure, the porous network of the pressed region collapses that results in decreased porosity, permeability and thickness. Then, the flow rate at the pressed region decreases according to the Darcy's law which means that the quantity of fluids that pass through the pressed region decreases according to the decreased permeability and thickness of the pressed region [32]. Therefore, as the amount of applied pressure increases, the time to wick the left dried region of the porous network increases, resulting in a delayed flow. Previously, we have calibrated delayed flow in a pressed NC membrane strip without any cover layers [31]. However, to integrate the pressed paper into a 3D paper-based microfluidic device, the pressed paper should be sandwiched between double sided tapes. Therefore, to confirm the possibility of the pressed paper to be applied to a 3D paper-based microfluidic device for inducing a delayed flow, we made a simple 3D paper-based microfluidic device (Fig. 3A). The pressed paper

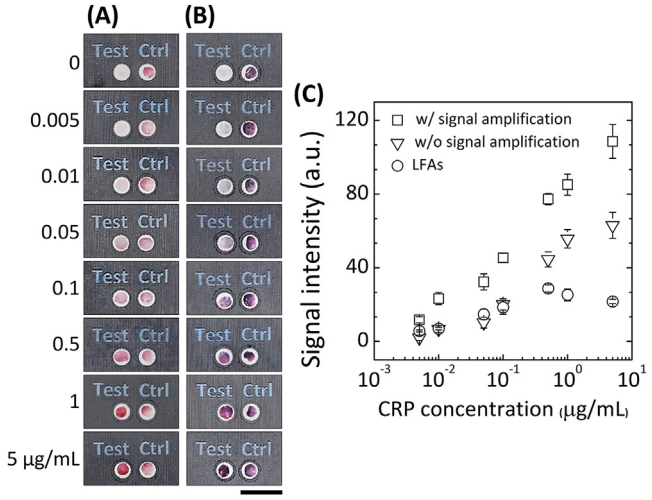

Fig. 4. hs-CRP detection results. The picture of the analysis region (8th layer) in a pressed region integrated 3D paper-based microfluidic device for VFAs (A) with and (B) without signal amplification. Scale bar = 5 mm. (C) The signal intensity of the test regions in conventional LFAs, VFAs without signal amplification, and VFAs with signal amplification was analyzed with respect to increasing concentration of CRP.

was placed between double sided tapes and blue dye was dried at the paper disk. The blue dye is rehydrated when the fluid reaches at the paper disk so that a blue color would appear in the outlet. Finally, according to increasing the amount of applied pressure, the time that the blue color appeared in the outlet was measured after loading of distilled water into the inlet (Fig. 3B). Although the pressed paper was sandwiched between double sided tapes, the wicking time increased with respect to increasing the amount of applied pressure (Fig. 3C). Therefore, the pressed paper can be used for delayed flow in a 3D paper-based microfluidic device for VFAs with multistep reactions. The time delay can also be achieved by controlling the position and length of the pressed region because the capillary flow is delayed after the pressed region. However, we did not apply an adjustment of the position and length of the pressed region since these methods are spatially limited that cannot achieve a large amount of time delay with limited dimensions of the device. Nevertheless, it is expected that a precise control of the time delay can be realized by adjusting the pressing pressure, the position, and the length of the pressed region.

3.3. *VFAs with multistep reactions for hs-CRP detection*

Based on the calibration results of the delayed flow, we designed a 3D paper-based microfluidic device containing the pressed region for VFAs with multistep reactions. Prepared gold enhancer solution should flow in the last order after target analytes and Ab conjugated AuNPs flow sequentially into the analysis region. If the prepared gold enhancer solution starts flowing into the analysis region before all of Ab conjugated AuNPs, a mixture of prepared gold enhancer solution and Ab conjugated AuNPs generate an abnormal signal in the analysis region (data not shown). It took about 170.67 ± 19.04 s for all the reagents from the inlets 1 and 2 flow sequentially into the analysis region, so that we selected the sufficient amount of applied pressure for the pressed region as 49.2 MPa based on the calibration result. First, various concentrations of CRP without signal amplification were detected by injecting PBS as a washing buffer into the inlet 3 instead of the prepared gold enhancer solution (Fig. 4A). The signal intensity of test region increased with respect to increasing concentration of CRP and the detection limit was about 0.01 μg/mL. The signal intensity was comparable to that of LFAs up to 0.5 μg/mL, but the signal intensity of the test lines in LFAs decreased over 0.5 μg/mL CRP concentration due to the Hook effect while the signal intensity of the test regions did not decrease (Fig. S5). Additionally, the signal intensity of the control region showed less deviation according to the concentration of CRP, although the signal intensity of the control region in LFAs changed according to the concentration of CRP due to line interference. It is expected that a more uniform signal at the control region would be helpful in assessing good operation of the device.

On the other hand, there was no background signal in the test region against 0 μg/mL CRP without washing step, indicating that no additional washing step is required for removing the background signal (Fig. S6). It can be understood that the remaining volume of the rehydration buffer into the inlet 2 plays a role as a washing buffer after the rehydration of Ab conjugated AuNPs. Therefore, we decided to detect various concentrations of CRP with signal amplification by loading prepared gold enhancer solution immediately after the injection of Ab conjugated AuNPs (Fig. 4B). According to the instruction of a gold enhancer solution, it is recommended to use a gold enhancer solution immediately after mixing each component. On the other hand, the prepared gold enhancer solution initiates to flow into the analysis region about 4 min after being loaded into the inlet 3. Although the prepared gold enhancer solution did not flow immediately into the analysis region after mixing each component, the signal intensity of the test region was a maximum of 3.47 times as compared to the results without signal amplification, resulting in an improved detection limit of about 0.005 μg/mL. However, the mixing process of each component to prepare the gold enhancer solution may complicate the reagent loading procedures. We expect it to be improved by storing each component of the gold enhancer in the dried state and rehydrating them with buffer [33].

Compared with the results of LFAs, we were able to successfully detect CRP in a clinically relevant range (0.005–5 μg/mL) for predicting the riskiness of cardiovascular disease without Hook effect (Fig. 4C). It is meaningful noting that the detection range can be widen by improving both the upper limit and the detection limit. There was no Hook effect because the detection conjugates pass through the test region after CRP is captured at the test region. Although the detection range of LFAs is expected to be adjusted by controlling the amount of detection conjugates, sample volume, and capture Abs, LFAs cannot detect a wide range of target analytes due to the Hook effect. In addition, even though the signal amplification step was added to the VFAs, the complicated operation principle has been simplified by maintaining the advantages of VFAs. The signal intensity of the test region may be saturated at high concentration of target analytes, but the high concentration of target analytes cannot be misread into a low concentration since there is no Hook effect. Because each layer of the 3D paper-based microfluidic device was manually aligned by adjusting the edge of each layer, there would be a quite large inter-device variation. The coefficient of variation (CV) was calculated to be 9.1%, 14.3%, 14.1%, 13.4%, 5.5%, 3.9%, 6.7%, and 8.5% with respect to increasing concentration of CRP from 0 to 5 μg/mL. Based on the calculated CV, it can be understood that a misalignment of each layer can cause a larger variation of assays at a low concentration of CRP rather than a high concentration of CRP. Since the signal intensity is small at a low concentration of CRP, a small change in the signal intensity that caused by a misalignment of each layer can have a large effect. The inter-device variation can be improved by integrating align marks at each layer or using the origami method for connecting each layer instead of double-sided tapes [25]. Furthermore, we expect that the 3D paper-based microfluidic device can be easily modified into a multiple detection format by simply modifying the geometry of the paper channel (Fig. S7). There would be no interferences between the test regions, because the reagents pass through the each test region independently.

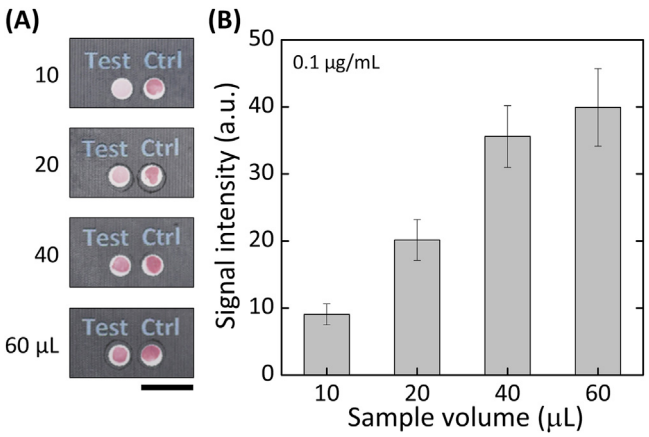

Fig. 5. The effect of sample volume. (A) The picture of the analysis region (8th layer) without signal amplification according to the amount of sample volume that detected 0.1 μg/mL CRP. Scale bar = 5 mm. (B) The signal intensity of the test region in panel A was plotted.

3.4. The effect of sample volume

In a pressed region integrated 3D paper-based microfluidic device for VFAs with multistep reactions, the reagents from the inlets 2 and 3 initiate to flow after all of the reagent from the inlet 1 flow into the analysis region. If the sample volume changes, the quantity of target analytes changes so that the signal intensity can be different for the same concentration of target analytes. Therefore, accurate sample volume should be loaded for reliable result assays. In this work, 20 μL of sample volume was used to achieve comparable results with LFAs to 0.5 μg/mL, but the signal intensity was changed according to the various amounts of sample volume (10, 20, 40, and 60 μL) with the same concentration of target analytes (0.1 μg/mL) without signal amplification. As shown in Fig. 5, the signal intensity increased with respect to the increasing amount of sample volume. However, it was difficult to handle over 60 μL of the sample volume due to the current dimension of the device. The signal intensity would be saturated at large sample volume, but CRP was successfully detected in the range from 0.005 to 5 μg/mL with a sample volume of 20 μL.

4. Conclusions

In this work, VFAs with multistep reactions were performed in a 3D paper-based microfluidic device based on a programmed reagent loading by utilizing a pressed paper. Delayed flow was achieved in a 3D paper-based microfluidic device based on a geometry modification of the paper channel and the utilization of the pressed region for the programmed reagent loading. The complicated operation principle of VFAs, requiring manual sequential loading of multiple reagents, was simplified by simultaneously loading all the reagents and programming their delivery order. However, the simultaneous loading of multiple reagents can be inconvenient for outside the laboratory environment. It can be improved by utilizing customized multi outlet pipette that stores all the reagents required for assays for commercialization. Additionally, we successfully performed hs-CRP detection that required for prediction of cardiovascular disease risk in the clinically relevant range within 15 min. It is meaningful that the sensitivity as well as the upper limit of assays were increased in VFAs with multistep reactions. In this sense, it is expected that the 3D paper-based microfluidic device for VFAs with multistep reactions would be more beneficial than LFAs for the detection of a wide range of target analytes. Furthermore, it can be simply developed into a multiple detection format by modifying the geometry of the paper channel so that the risk of cardiovascular disease can be predicted with combination of other biomarkers for cardiovascular disease such as cardiac troponin I and myoglobin.

Acknowledgments

This research was supported by a Mid-Career Researcher Program (Grant No. NRF-2016R1A2B3015986), a Bio & Medical Technology Development Program (Grant No. NRF-2015M3A9B3028685), and a NRF-2016-Global Ph.D. Fellowship Program through the National Research Foundation (NRF) of Korea funded by the Ministry of Science, ICT and Future Planning.

Appendix A. Supplementary data

Supplementary data associated with this article can be found, in the online version, at http://dx.doi.org/10.1016/j.snb.2017.02.150.

References

[1] G.P. Castelli, C. Pognani, M. Meisner, A. Stuani, D. Bellomi, L. Sgarbi, Procalcitonin and C-reactive protein during systemic inflammatory response syndrome, sepsis and organ dysfunction, Crit. Care 8 (2004) 1.
[2] T.B. Ledue, N. Rifai, Preanalytic and analytic sources of variations in C-reactive protein measurement: implications for cardiovascular disease risk assessment, Clin. Chem. 49 (2003) 1258–1271.
[3] T.A. Pearson, G.A. Mensah, R.W. Alexander, J.L. Anderson, R.O. Cannon, M. Criqui, Y.Y. Fadl, S.P. Fortmann, Y. Hong, G.L. Myers, Markers of inflammation and cardiovascular disease application to clinical and public health practice: a statement for healthcare professionals from the centers for disease control and prevention and the American Heart Association, Circulation 107 (2003) 499–511.
[4] J.L. Clarke, J.L. Anderson, J.F. Carlquist, R.F. Roberts, B.D. Horne, T.L. Bair, M.J. Kolek, C.P. Mower, A.M. Crane, W.L. Roberts, J.B. Muhlestein, Comparison of differing C-reactive protein assay methods and their impact on cardiovascular risk assessment, Am. J. Cardiol. 95 (2016) 155–158.
[5] R. Dominici, P. Luraschi, C. Franzini, Measurement of C-reactive protein: two high sensitivity methods compared, J. Clin. Lab. Anal. 18 (2004) 280–284.
[6] W.-B. Lee, Y.-H. Chen, H.-I. Lin, S.-C. Shiesh, G.-B. Lee, An integrated microfluidic system for fast, automatic detection of C-reactive protein, Sens. Actuators B Chem. 157 (2011) 710–721.
[7] Y.-N. Yang, H.-I. Lin, J.-H. Wang, S.-C. Shiesh, G.-B. Lee, An integrated microfluidic system for C-reactive protein measurement, Biosens. Bioelectron. 24 (2009) 3091–3096.
[8] R.K. Gupta, A. Periyakaruppan, M. Meyyappan, J.E. Koehne, Label-free detection of C-reactive protein using a carbon nanofiber based biosensor, Biosens. Bioelectron. 59 (2014) 112–119.
[9] S.K. Vashist, E.M. Schneider, R. Zengerle, F. von Stetten, J.H. Luong, Graphene-based rapid and highly-sensitive immunoassay for C-reactive protein using a smartphone-based colorimetric reader, Biosens. Bioelectron. 66 (2015) 169–176.
[10] A.K. Yetisen, M.S. Akram, C.R. Lowe, Paper-based microfluidic point-of-care diagnostic devices, Lab Chip 13 (2013) 2210–2251.
[11] X. Mao, Y. Ma, A. Zhang, L. Zhang, L. Zeng, G. Liu, Disposable nucleic acid biosensors based on gold nanoparticle probes and lateral flow strip, Anal. Chem. 81 (2009) 1660–1668.
[12] H.-A. Joung, Y.K. Oh, M.-G. Kim, An automatic enzyme immunoassay based on a chemiluminescent lateral flow immunosensor, Biosens. Bioelectron. 53 (2014) 330–335.
[13] Y.K. Oh, H.-A. Joung, H.S. Han, H.-J. Suk, M.-G. Kim, A three-line lateral flow assay strip for the measurement of C-reactive protein covering a broad physiological concentration range in human sera, Biosens. Bioelectron. 61 (2014) 285–289.
[14] T. Senthilkumar, M. Subathra, M. Phil, P. Ramadass, V. Ramaswamy, Rapid serodiagnosis of leptospirosis by latex agglutination test and flow-through assay, Indian J. Med. Microbiol. 26 (2008) 45.
[15] L. Sibanda, S. De Saeger, I. Barna-Vetro, C. Van Peteghem, Development of a solid-phase cleanup and portable rapid flow-through enzyme immunoassay for the detection of ochratoxin A in roasted coffee, J. Agric. Food Chem. 50 (2002) 6964–6967.
[16] S.A. Fernando, G.S. Wilson, Studies of the 'hook' effect in the one-step sandwich immunoassay, J. Immunol. Methods 151 (1992) 47–66.
[17] Y.K. Oh, H.-A. Joung, S. Kim, M.-G. Kim, Vertical flow immunoassay (VFA) biosensor for a rapid one-step immunoassay, Lab Chip 13 (2013) 768–772.
[18] J.E. Schonhorn, S.C. Fernandes, A. Rajaratnam, R.N. Deraney, J.P. Rolland, C.R. Mace, A device architecture for three-dimensional, patterned paper immunoassays, Lab Chip 14 (2014) 4653–4658.
[19] G.E.N. Pauli, A. de la Escosura-Muñiz, C. Parolo, I.H. Bechtold, A. Merkoçi, Lab-in-a-syringe using gold nanoparticles for rapid immunosensing of protein biomarkers, Lab Chip 15 (2015) 399–405.

[20] T. Liang, R. Robinson, J. Houghtaling, G. Fridley, S.A. Ramsey, E. Fu, Investigation of reagent delivery formats in a multivalent malaria sandwich immunoassay and implications for assay performance, Anal. Chem. 88 (2016) 2311–2320.
[21] A. Apilux, Y. Ukita, M. Chikae, O. Chailapakul, Y. Takamura, Development of automated paper-based devices for sequential multistep sandwich enzyme-linked immunosorbent assays using inkjet printing, Lab Chip 13 (2013) 126–135.
[22] C.A. Grant, K. Smith, Highly sensitive two-dimensional paper network incorporating biotin–streptavidin for the detection of malaria, Anal. Chem. 88 (2016) 2553–2557.
[23] P. He, I. Katis, R. Eason, C.L. Sones, Engineering fluidic delays in paper-based devices using laser direct-writing, Lab Chip 15 (2015) 4054–4061.
[24] A.W. Martinez, S.T. Phillips, G.M. Whitesides, Three-dimensional microfluidic devices fabricated in layered paper and tape, Proc. Natl. Acad. Sci. U. S. A. 105 (2008) 19606–19611.
[25] L. Ge, S. Wang, X. Song, S. Ge, J. Yu, 3D origami-based multifunction-integrated immunodevice: low-cost and multiplexed sandwich chemiluminescence immunoassay on microfluidic paper-based analytical device, Lab Chip 12 (2012) 3150–3158.
[26] G.G. Lewis, M.J. DiTucci, M.S. Baker, S.T. Phillips, High throughput method for prototyping three-dimensional, paper-based microfluidic devices, Lab Chip 12 (2012) 2630–2633.
[27] B. Kalish, H. Tsutsui, Patterned adhesive enables construction of nonplanar three-dimensional paper microfluidic circuits, Lab Chip 14 (2014) 4354–4361.
[28] H. Noh, S.T. Phillips, Fluidic timers for time-dependent, point-of-care assays on paper, Anal. Chem. 82 (2010) 8071–8078.
[29] K.N. Han, J.-S. Choi, J. Kwon, Three-dimensional paper-based slip device for one-step point-of-care testing, Sci. Rep. 6 (2016) 25710.
[30] J.H. Shin, J. Park, S.H. Kim, J.-K. Park, Programmed sample delivery on a pressurized paper, Biomicrofluidics 8 (2014) 054121.
[31] J. Park, J.H. Shin, J.-K. Park, Pressed paper-based dipstick for detection of foodborne pathogens with multistep reactions, Anal. Chem. 88 (2016) 3781–3788.
[32] J. Park, J.H. Shin, J.-K. Park, Experimental analysis of porosity and permeability in pressed paper, Micromachines 7 (2016) 48.
[33] E. Fu, T. Liang, P. Spicar-Mihalic, J. Houghtaling, S. Ramachandran, P. Yager, Two-dimensional paper network format that enables simple multistep assays for use in low-resource settings in the context of malaria antigen detection, Anal. Chem. 84 (2012) 4574–4579.

Biographies

Juhwan Park received his BS and MS degrees in bio and brain engineering from the Korea Advanced Institute of Science and Technology (KAIST) in 2014 and 2016, respectively. He is currently a Ph.D. candidate in the Department of Bio and Brain Engineering, KAIST. His current research interests include microfluidics, lab on a chip, and bioMEMS.

Je-Kyun Park is a Professor of Bio and Brain Engineering at the KAIST. He received his Ph.D. degree in biotechnology from the KAIST in 1992. Prior to joining KAIST, he worked as a Postdoctoral Research Fellow in the Department of Biomedical Engineering at the Johns Hopkins University School of Medicine in the USA (1996–1997) and as Chief Research Engineer at the LG Electronics Institute of Technology in Korea (1992–2002). He was an editorial board member of several international journals, including Lab on a Chip, Biosensors and Bioelectronics, and BioChip Journal. He is co-author of 8 book chapters, 113 patents, and more than 140 peer-reviewed scientific papers in the field of integrative bioengineering, including nanobiotechnology, bioMEMS for cell/tissue engineering, and lab-on-a-chip & microfluidic analytical technologies.